Chemically modified STM tips for atomic-resolution imaging on ultrathin NaCl films

Zhe Li, Koen Schouteden, Violeta Iancu, Ewald Janssens, Peter Lievens, Chris Van Haesendonck*

Solid-State Physics and Magnetism Section, KU Leuven, BE-3001 Leuven, Belgium

Jorge I. Cerdá †

Instituto de Ciencia de Materiales, ICMM-CSIC, Cantoblanco, 28049 Madrid, Spain

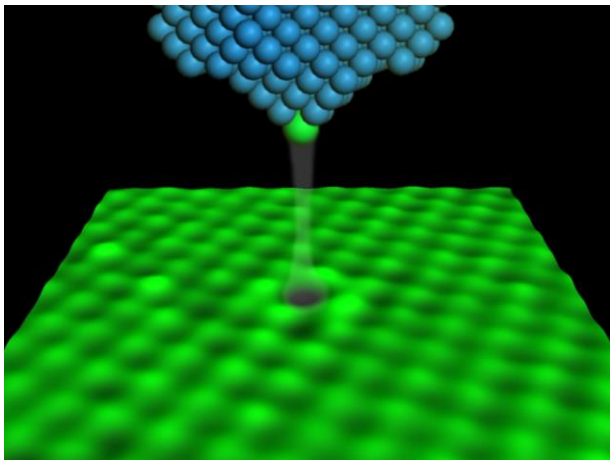

The chemically modified STM-tip is obtained by picking up a Cl ion from the NaCl surface. With respect to the bare metal tip, the Cl-functionalized tip yields an enhanced resolution accompanied by a contrast reversal in the STM topography image.

Peter Lievens, http://fys.kuleuven.be/vsm/class/
Chris Van Haesondonck, http://fys.kuleuven.be/vsm/spm/
Jorge I. Cerdá, http://www.icmm.csic.es/jcerda/

Nano Research
DOI (automatically inserted by the publisher)
Research Article
ISSN 1998-0124
CN 11-5974/O4

Chemically modified STM tips for atomic-resolution imaging on ultrathin NaCl films

Zhe Li, Koen Schouteden, Violeta Iancu, Ewald Janssens, Peter Lievens, Chris Van Haesendonck (✉)

Solid-State Physics and Magnetism Section, KU Leuven, BE-3001 Leuven, Belgium

Jorge I. Cerdá (✉)

Instituto de Ciencia de Materiales, ICMM-CSIC, Cantoblanco, 28049 Madrid, Spain

Received: day month year
Revised: day month year
Accepted: day month year (automatically inserted by the publisher)

KEYWORDS

Scanning tunneling microscopy, ultrathin insulating films, functionalized STM-tip, STM simulation

ABSTRACT

Cl-functionalized tips for scanning tunneling microscopy (STM) are obtained by in situ modifying a tungsten STM-tip on islands of ultrathin NaCl(100) films on Au(111) surfaces. The functionalized tips achieve a neat atomic resolution imaging of the NaCl(100) islands. With respect to bare metal tips, the chemically modified tips yield a drastically enhanced spatial resolution as well as a contrast reversal in the STM topography images, implying that Na atoms instead of Cl atoms are imaged as protrusions. STM simulations based on a Green's function formalism explain the experimentally observed contrast reversal in the STM topography images as due to the highly localized character of the Cl-p_z states at the tip apex. An additional remarkable characteristic of the modified tips is that in dI/dV maps a Na atom appears as a ring with a diameter that depends crucially on the tip-sample distance.

The chemical termination of the tip apex in scanning tunneling microscopy (STM) experiments determines the interaction between the wave functions of the tip and those of the sample and hence the resolution that can be achieved in STM images. For example, it has been demonstrated that a molecule-terminated STM tip yields high-resolution molecular-orbital imaging due to the p-orbital character of the tip apex, far superior to what is achieved with a bare metal tip [1, 2]. Atomic resolution imaging is of utmost importance for the manipulation and investigation of surface

Address correspondence to Chris Van Haesendonck, chris.vanhaesendonck@fys.kuleuven.be; Jorge I. Cerdá, jcerda@icmm.csic.es

point defects and adatoms, as well as for the determination of the atomic structures of molecules and nanoparticles [3-6].

Ultrathin insulating films grown on conductive substrates effectively reduce the electronic coupling between deposited nanoparticles and their metallic support and are therefore ideally suited for local probe based investigations. This way, the intrinsic electronic properties of atoms [7], molecules [8, 9], and clusters [10], as well as charge [11, 12] and spin [13-15] manipulations of single atoms have been investigated on different ultrathin insulating films, including magnesium oxide, sodium chloride, and copper nitride. Among these insulating materials, NaCl has the advantage that it can be grown as atomically flat layers on various metal surfaces [16-19] and that the thickness of the layers can be tuned [20]. Previous STM experiments have reported atomic resolution on ultrathin NaCl films in STM topography images [16, 19, 21]. Via density functional theory (DFT) based calculations in the Tersoff-Hamann approximation it has been found that the protrusions observed in the topography images using a bare metal tip are Cl atoms, while the Na atoms cannot be resolved [16, 21]. Recently, we showed that simultaneous visualization of both atomic species of (bilayer) NaCl on Au(111) can be achieved in the local hcp regions of the Au(111) surface reconstruction in the dI/dV maps using a Cl-functionalized tip [22]. We also illustrated that such tips can be used to probe the surface of (hemi)spherical nanoparticles [i.e., Co clusters deposited on NaCl(100)/Au(111)] with atomic resolution, which could not be achieved with a bare metal STM tip [23]. In Refs. [22] and [23], functionalization of the STM tip was only occasionally obtained by uncontrolled picking up of a Cl ion during repeated scanning of the NaCl surface in close proximity, thereby hampering more challenging systematic investigations.

Various experiments with controlled functionalization of the STM tips have been reported before [1, 2, 24]. To obtain such tips, it was required to introduce "impurity" molecules, such as CO, O_2, and H_2, on the sample, which can be picked up by the STM tip to achieve functionalization and enhanced resolution. When investigating the properties of nanoparticles, especially metal nanoparticles, the adsorption of CO, O_2 or H_2 molecules on the sample may result in unwanted reactions with the nanoparticles and modify their properties. Therefore, it would be advantageous if the STM tip can be conveniently functionalized with a species that is available on the clean substrate surface, without the need to introduce extra impurity molecules.

Here, we demonstrate that chemically modified STM tips can be controllably obtained on ultrathin NaCl(100) films on Au(111) by bringing the tip into contact with the NaCl surface via current-distance spectroscopy. Using such Cl-functionalized tips, atomic resolution of mono-, bi-, and trilayer NaCl islands is routinely achieved in STM topography images as well as in constant-current dI/dV maps. We find that the resolution and the appearance of the atoms in such dI/dV maps depend crucially on the tip-sample distance, which can be related to a different overlap of the tip and sample wave functions at different tip-sample distances. Theoretical STM simulations based on a Green's function formalism reveal that the observed drastic enhancement of the contrast as well as the contrast reversal in the topography images can be explained by the Cl-termination of the STM tip apex.

NaCl layers are grown using vapor deposition at 800 K in the preparation chamber of the STM setup (Omicron Nanotechnology) in ultra-high vacuum (UHV). Monolayer and bilayer NaCl(100) islands are formed when, during the NaCl deposition, the Au(111) substrate is kept cold or at room temperature, respectively. Subsequent annealing of the sample to 460 K yields trilayer NaCl(100) islands [20]. The STM measurements are performed in UHV (10^{-11} mbar) and at low temperature (T_{sample} = 4.5 K). Tunneling voltages are always given for the sample, while the STM tip is virtually grounded. All dI/dV maps are acquired with a closed feedback loop using tunneling voltage modulation (amplitude of 50 mV and frequency around 800 Hz) and lock-in amplification based detection. Image processing is performed by Nanotec WSxM [25].

Figure 1(a) illustrates the effect of the modified STM tip on the resolution of STM topography images of trilayer NaCl(100) on Au(111). Modification is controllably achieved by bringing the tungsten STM tip into contact with the NaCl surface via current-distance $I(z)$ spectroscopy. It can be seen in Fig. 1(a) that a drastic enhancement of the resolution occurred after the $I(z)$ spectrum was

recorded near the middle of the image. The lower part is imaged with the bare W tip and exhibits rather poor atomic resolution, whereas in the upper part the atomic structure of the surface can be clearly resolved with a modified tip [see Supplementary Material (SM) for more details]. As evidenced below, we assign the enhancement of the resolution to picking up a Cl ion by the STM tip upon contact with the NaCl surface. The transfer of the Cl ion from the surface to the tip most probably occurs due to an increasing overlap between the potential wells associated with Cl adsorption on tip and sample as they approach each other [26]. For sufficiently close distances the two wells will merge into a single one and further retraction of the tip under an applied bias may then favor the attachment of the Cl to the tip apex.

Indeed, we find that a surface defect is always created in the NaCl film after the tip modification. However, the defect appears to extend to four neighboring atom sites, as illustrated in Figs. 1(b)-(d). Remarkably, the appearance of the defect changes drastically after the STM tip has lost its functionalization, which can spontaneously occur during scanning. When using a bare W tip, the defect appears as an atomic size vacancy in the NaCl film as can be seen in Fig. 1(e). Such vacancies have previously been reported for the case of NaCl(100) films on Cu(111) and they were identified as missing Cl ions in the NaCl film, also referred to as Cl vacancies [19]. The observed change in the appearance of the defect indicates that contrast reversal occurs in STM topography images that are recorded with the modified tip when compared to the bare W tip. This contrast reversal implies that the modified tip images the Cl^- ions as depressions and the Na^+ ions as protrusions. Simulations of the STM topography images (discussed below) confirm that the contrast reversal is indeed induced by the Cl termination of the W tip.

Figures 1(b)-(d) presents a series of STM topography images recorded with increasing current from 0.1 nA to 0.32 nA at a fixed negative sample voltage V = −0.8 V. It can be seen that the Na^+ ions appear larger with increasing current and that at the same time the image contrast decreases. The corrugations are 45 pm in Fig. 1 (b), 42 pm in Fig. 1 (c) and 35 pm in Fig. 1 (d), where the main contribution to the corrugation stems from the Au(111) herringbone reconstruction.

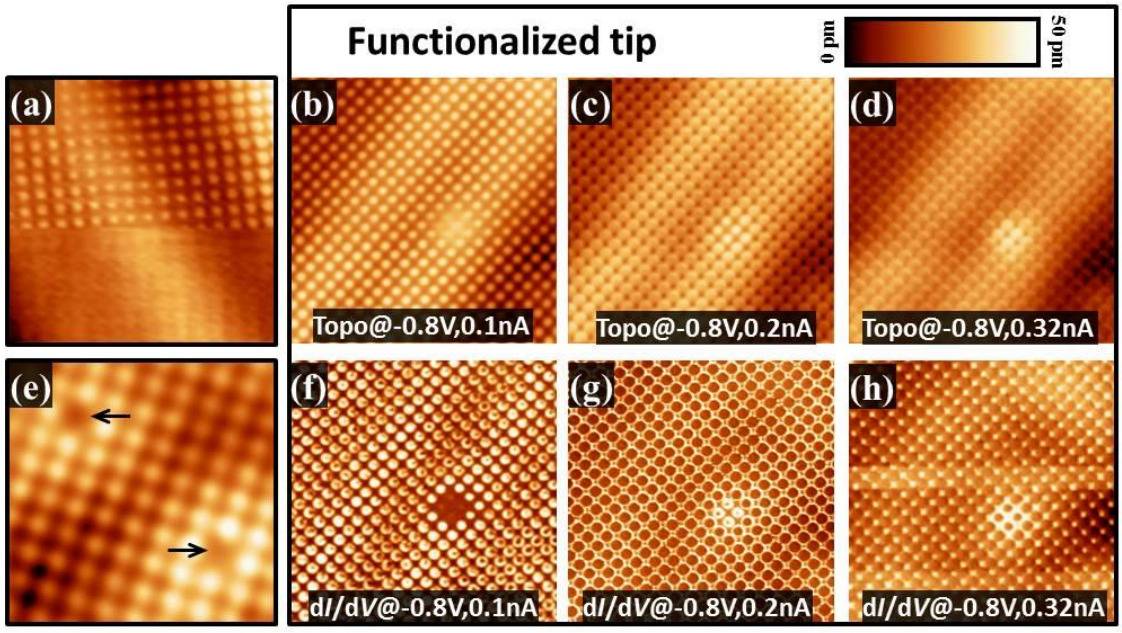

Figure 1. (a) 6.3×6.3 nm^2 STM topography image illustrating the influence of the tip modification on the imaging resolution, which is drastically enhanced after bringing the STM tip into contact with the NaCl surface (V = −1.0 V, I = 0.2 nA). (b)-(d) 8×8 nm^2 STM topography image recorded with a modified tip at the same tunneling voltage of −0.8 V, and with different current of 0.1 nA, 0.2 nA, and 0.32 nA, respectively. The surface exhibits a defect that can be assigned to a single Cl vacancy. The color bar indicates the z amplitudes of 46 pm, 42 pm and 35 pm for the topography images in (b)-(d), respectively. (e) 3.4×3.4 nm^2 STM topography image of two Cl vacancies (indicated by the black arrows) recorded at V = −0.8 V and I = 0.16 nA using a bare W tip. (f)-(h) Corresponding 8×8 nm^2 dI/dV maps of (b)-(d).

To confirm that the modified tip is terminated by a Cl atom and to gain further insight into the mechanism of the contrast reversal in topography images, we carried out simulations of the STM topography with a Green's function based formalism that treats the tip on the same footing as the sample surface, thus allowing to investigate the effect of different tip terminations. We considered two differently oriented bare W tips [W(110) and W(111)], two Cl-functionalized tips of which one oriented along the W(110) direction [denoted as W(110)-Cl] and the other one along the (111) direction of a hypothetical W *fcc* phase [denoted as W(111)-Cl] [27], as well as a Na-terminated tip [W(110)-Na]. The surface was modeled as a NaCl(100) trilayer on top of the Au(111) surface. As depicted in Fig. 2(a), to describe the surface we employed a large c(10×10) NaCl(100) trilayer commensurate with a $\begin{pmatrix} 11 & 3 \\ 3 & 11 \end{pmatrix}$ Au(111) supercell after slightly distorting the Au lattice. All simulations were performed with the GREEN package [28, 29], using the extended Hückel theory (EHT) [30, 31] to describe the electronic structure of both the sample and tip (details of the calculation parameters as well as the resulting Au and NaCl electronic structures are given in the SM).

Figures 2(b)-(d) present topography images simulated at $V = -0.8$ V using different tip models as described above. The bare W [W(110) and W(111)] tips [see Fig. 2(b) and Fig. S10 in the SM, respectively] and the Na-terminated tip (see Fig. S11 in the SM) result in a weaker corrugation with maxima at the Cl atoms for different tunneling current. On the other hand, the W(110)-Cl [Fig. 2(c)] and W(111)-Cl tips [Fig. S13(b)] result in well resolved bumps on top of the Na atoms at relatively low currents. Moreover, the W(110)-Cl tip resolves both species for particular tunneling parameters [Fig. 2(d)]; however, decreasing the tip-sample distance (i.e., using larger currents) shifts the maxima to the Cl atoms, while increasing the tip-sample distance yields the maxima on the Na atoms [Fig. 2(c)]. Note that in Fig. 2d there is a clear symmetry breaking with respect to the expected *pmm* one (after combining the NaCl's 4-fold and tip's *pmm* symmetries) induced by the underlying Au substrate. Such asymmetric features only become visible at gap resistances where both species are resolved and for this particular tip [see, for instance, Fig. S13(b) where the 3-fold W(111)-Cl tip yields highly symmetric images]. Also note that although the large size of the supercell used to model the surface may account to some extent for the incommensurability between the square NaCl(100) and hexagonal Au(111) lattices, it is still too small to accommodate the Au(111) herringbone reconstruction [32], which causes large-scale modulations in the images (see for instance the variations between fcc and hcp regions of the Au(111) surface in Figs. S3 and S4 and the corresponding discussion in the SM). We therefore restrict the theoretical analysis below to the explanation of the origin of the contrast reversal induced by the adsorbed Cl in the topographic images since this effect can be clearly seen in all regions of the sample.

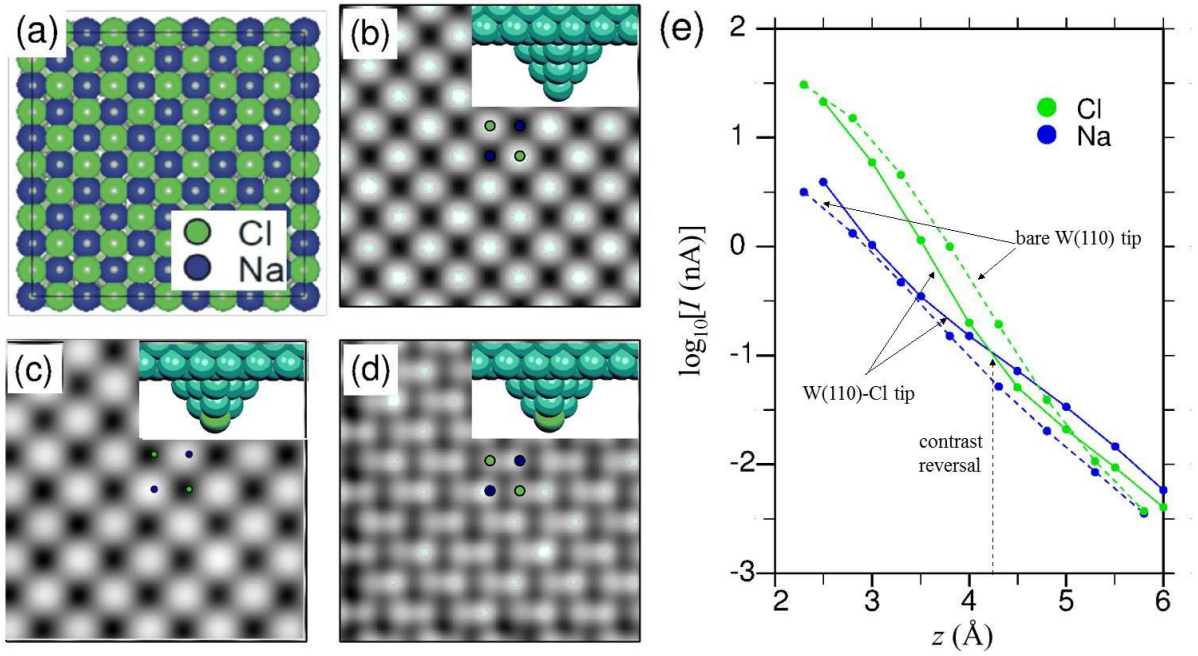

Figure 2. (a) Top view of the trilayer NaCl(100) on Au(111) model used in the simulation. Simulated STM topography at V = −0.8 V, (b) using a bare W(110) tip image at I = 0.1 nA, (c) and (d) using a Cl-terminated W(110) tip at I = 0.02 nA ($\log_{10}I \approx -1.7$) and I = 0.1 nA ($\log_{10}I$ = −1.0), respectively . The dark green and blue circles represent Cl atoms and Na atoms, respectively. (e) $I(z)$ curves calculated at V = −0.8 V for the bare W(110) (dashed lines) and W(110)-Cl (solid lines) tips placed on top of a Na atom (blue) and on top of a Cl atom (green), respectively. The points are calculated while the lines are only a guide to the eye.

Figure 2(e) presents simulated $I(z)$ curves for a bare W(110) tip and a W(110)-Cl tip with the tip apex placed above a Na and above a Cl atom, respectively. The simulated $I(z)$ curves for a W(111)-Cl tip are similar to those for the W(110)-Cl tip [see Fig. S13(a) in the SM]. For the bare tip (dashed lines), the current decays faster with the tip-sample distance z above a Cl atom than above a Na atom, but is always larger above a Cl atom. For the Cl-functionalized tip (solid lines), a larger slope of the $I(z)$ curve is found above a Cl atom but only at smaller tip-sample distances. At $z \approx 4.2$ Å (corresponding to I ≈ 0.1 nA) the currents above a Na atom and above a Cl atom become equal and a contrast reversal occurs as the tip is further retracted. For $z > 4.2$ Å Na should then be revealed in the topography image. Below the contrast reversal point [i.e. the point where the $I(z)$ curves above the Na and above the Cl cross], the contrast between Na and Cl first rather rapidly increases with decreasing current, which is consistent with our experimental observations [Figs. 1(b)-(d)], indicating that the tunneling conditions for Figs. 1(b)-(d) are close to the contrast reversal point. However, when further decreasing the current, i.e. at large tip-sample distances, the contrast will start to gradually decrease with decreasing current and the $I(z)$ curves above the Na and above the Cl will ultimately coincide as expected for $z >> 4.2$ Å. This decrease of contrast with decreasing current for low currents is experimentally confirmed in Figs. S3(a) and (b) in the SM, which indicates that the tunneling conditions in that case are considerably below the contrast reversal point. The trends described above are the same for a W(111)-Cl tip (see $I(z)$ curves in Fig. S13 in the SM).

For positive voltages, the behavior of the $I(z)$ curves is similar to the behavior observed at negative voltages. On the other hand, the exact point of contrast reversal is different. Figure S5(a) in the SM reveals that the contrast in experimental topography images increases with increasing current at a fixed positive voltage, which is corroborated by the simulations (see Fig. S12 in the SM). All these results consistently explain the experimental findings and confirm that the functionalized tips indeed are terminated by a Cl atom.

A decomposition of the simulated current into tunneling paths (data not shown) reveals that the major contributions to the current always involve the p_z orbitals of the Na or Cl atoms at the surface.

However, as illustrated in Fig. S8(a) and Table S1 in the SM, there is a large difference in the level of localization of these orbitals between both elements, with those of Na much more extended than the Cl ones. Hence, the current decays faster at the Cl sites (i.e., larger $I(z)$ slope) than at the Na sites. For the Cl-terminated tip, the p-orbitals of the Cl apex dominate the tunneling current for our experimental measurement conditions (tunneling voltage and current range), while other states, including the W d-orbitals, only have a minor contribution to the tunneling current. In case the terminated Cl tip is positioned above a Cl atom, the overlap between its highly localized p_z orbitals decays so fast when $z > 4.2$ Å that the signal becomes smaller than at a Na site [Fig. 2(e)] and contributions from the more extended p_z orbitals of the neighboring Na atoms start to dominate the current. This explains both the contrast reversal and the similar $I(z)$ slopes at the Na and Cl sites found at large tip-sample distances for the Cl-terminated tips. A similar analysis for the W(111)-Cl tip leads to the same conclusions. On the other hand, for the bare tungsten tip, taking the W(110) tip for example, the contribution of the different states to the tunneling current depends on the precise location of the tip above the NaCl surface. When the W tip is located on top of a Cl atom of the NaCl surface, the main contributions from the W tip are W-$d_{x^2-y^2}$ (60%), W-p_z (27%), and W-s (10%), which all interact with the p_z orbital of the Cl atoms of the NaCl surface. However, when the tip is located on top of the Na atoms of the NaCl surface, we find a complex interplay between the different tip and Na states. The largest contributions to the tunneling current are W-s→Na-p_z (24%) and W-p_z→Na-s (15%). The remaining 60% contribution comes from a complex interference interplay between many different paths. Overall, the decay of the overlap between the Cl and W states with z is not sufficiently large to induce a contrast reversal even at the largest z values, in accordance with the experiments. We mention that apart from the pure electronic effects presented above, dynamical force sensor effects [33] may also play a role in the contrast reversal, although their influence should become more pronounced at small tip-sample distances.

We now turn to our experimentally measured constant-current dI/dV maps. While we achieved a good agreement between the measured and the simulated STM topography images for the high spatial resolution as well as for the contrast reversal, the constant-current dI/dV maps, which are conveniently recorded simultaneously with the topography images, present an additional remarkable characteristic of the modified tip that will be illustrated and discussed below. We would like to stress that for the constant-current dI/dV maps we do not aim at any comparison with simulated maps. First of all, full DFT based calculations of the local density of states (LDOS) probed by a Cl-terminated tip cannot be performed at this point. Also, dI/dV maps acquired under constant-height or open-feedback-loop conditions are more appropriate for comparing theory and experiment when focusing on the LDOS [34]. On the other hand, for the constant-height or open-feedback-loop conditions, our Cl-terminated tips do not survive for a sufficiently long time to perform a systematic study of the influence of the tunneling parameters on the spatial resolution. The spatial resolution for open-feedback-loop conditions turns out to be prone to fluctuations for detailed measurements that require longer measuring times.

Figures 1(f)-(h) present a series of dI/dV maps recorded at the location corresponding to the STM topography images of Figs. 1(b)-(d). The dI/dV maps are recorded at the same tunneling voltage of −0.8 V, but with different settings of the tunneling current. While in the corresponding STM topography images [Figs. 1(b)-(d)] only Na atoms are resolved as protrusions, independent of the tunneling current, in the dI/dV maps the appearance of the atoms depends strongly on the tunneling current, as illustrated in Figs. 1(f)-(h). Upon more careful comparison, it can be seen that the drastic changes in the constant-current dI/dV maps show a clear correlation with the more subtle contrast changes observed in the corresponding topography images. Remarkably, it can be seen that the brightest dI/dV features evolve from one atomic species (Na or Cl) to the other when changing the tunneling current. At lower current each Na atom appears as a ring-like feature in the dI/dV maps [Fig. 1(f)]. With increasing current, the diameter of the rings gradually increases [Fig. 1(g)] and the neighboring rings start to overlap until, at sufficiently high currents, the rings can no longer

be resolved and the highest dI/dV signal is found on the other atomic species, i.e., Cl [Fig. 1(h)].

Increasing/decreasing the current at a constant voltage [Figs. 1(f)-(h)] in fact decreases/increases the tip-sample distance. The above results therefore indicate that the appearance of the atoms in the dI/dV maps recorded with the modified tip depends mainly on the height of the STM tip above the NaCl surface or, equivalently, on the tunneling gap resistance. In particular, a contrast reversal in the dI/dV maps is found to occur at a specific tip-sample distance which in general varies from tip to tip due to changes in the apex geometries and/or the Cl adsorption sites. These trends in the dI/dV maps are the same for positive and negative sample voltages and in fact allow to identify if one is close to or far away from the contrast reversal point. At larger tip-sample distances (well below the contrast reversal point) Na is revealed as a dot [Figs. 1(f) and Fig. S3(d)], while at smaller tip-sample distances (near the contrast reversal point) it is revealed as a ring [Figs. 1(g)]. When approaching the tip further towards the NaCl surface (very close to the contrast reversal point), the ring-like features overlap and form a dot on the Cl sites [Fig. 1(h)].

Notably, the enhanced resolution and the reversal processes do not depend on the sign of the applied voltage, since similar results are obtained under positive biases (Fig. S5 in the SM). Regarding the film thickness, bilayer NaCl presents the same behavior (Fig. S6 in the SM), while for monolayer NaCl we only observe the enhancement in the topography images after the tip modification [35], but no ring structures in the dI/dV maps. We assign this absence to larger tip-sample distances when measuring with similar tunneling setpoints, since the monolayer film presents a much smaller electrical resistance than the bi- and trilayer films. Bare W tips, on the other hand, yield dI/dV maps with no or only very weak atomic resolutions (see Fig. S7 in SM), and hence a detailed comparison of the bias/current dependence with the modified tip is not feasible.

Occasionally, the modified tip is able to simultaneously image both the Na atoms and the Cl atoms in the dI/dV maps (Fig. S3 in the SM) as well as in the topography images (Fig. S4). Although the resolution obtained with the modified STM tips varies somewhat from tip to tip (see Fig. 1 and also Figs. S2-S4 in the SM), the main features are consistent: Na atoms are observed as ring-like features in the dI/dV maps with their diameter depending on the tip-sample distance.

In summary, tungsten STM tips were chemically modified on ultrathin NaCl(100) films, resulting in Cl-functionalized tips that are used to demonstrate atomic resolution imaging of NaCl(100) islands on Au(111). It was demonstrated that the modified STM tips enhance and reverse the contrast in STM topography images compared to a bare metal STM tip. Simulated STM images, which take into account the specific termination of the tip apex, demonstrate that the modified STM tips are indeed functionalized by a Cl atom. Cl-functionalized tips can be used for systematic high-resolution investigations of adsorbates, such as adatoms, molecules, and nanoclusters, on thin NaCl insulating films. The reported approach may be generalized to other thin films or semiconductor/oxide surfaces. We believe the key issue is to have an electronegative atom exposed at the surface. This should not necessarily be Cl as used in this study, but S or P also should improve the resolution. On the other hand, lighter electronegative elements such as oxygen or carbon present too highly localized orbitals and thus require smaller tip-sample distances in order to achieve the contrast reversal. In such regime, however, dynamical tip-sample interactions may become predominant and the interpretation of the data becomes less straightforward.

Acknowledgements

The research in Leuven has been supported by the Research Foundation – Flanders (FWO, Belgium) and the Flemish Concerted Action research program (BOF KU Leuven, GOA/14/007). Z. L. thanks the China Scholarship Council for financial support (No. 2011624021). K. S. and V. I. are postdoctoral researchers of the FWO. J. C. acknowledges financial support from the Spanish Ministry of Innovation and Science under contract NOs. MAT2010-18432 and MAT2013-47878-C2-R.

Electronic Supplementary Material: Supplementary Material (more details of the STM experiments and simulations) is available in the online version of this article at

http://dx.doi.org/10.1007/s12274-***-****-* (automatically inserted by the publisher).

References

[1] Gross, L.; Moll, N.; Mohn, F.; Curioni, A.; Meyer, G.; Hanke, F.; Persson, M. High-Resolution Molecular Orbital Imaging Using a p-Wave STM Tip. *Phys. Rev. Lett.* **2011,** *107*, 086101.

[2] Martínez, J. I.; Abad, E.; González, C.; Flores, F.; Ortega, J. Improvement of Scanning Tunneling Microscopy Resolution with H-Sensitized Tips. *Phys. Rev. Lett.* **2012,** *108*, 246102.

[3] Krasnikov, S.; Lübben, O.; Murphy, B.; Bozhko, S.; Chaika, A.; Sergeeva, N.; Bulfin, B.; Shvets, I. Writing with atoms: Oxygen adatoms on the MoO_2/Mo(110) surface. *Nano Res.* **2013,** *6*, 929-937.

[4] Lingley, Z.; Mahalingam, K.; Lu, S.; Brown, G.; Madhukar, A. Nanocrystal-semiconductor interface: Atomic-resolution cross-sectional transmission electron microscope study of lead sulfide nanocrystal quantum dots on crystalline silicon. *Nano Res.* **2014,** *7*, 219-227.

[5] Gross, L.; Mohn, F.; Moll, N.; Liljeroth, P.; Meyer, G. The Chemical Structure of a Molecule Resolved by Atomic Force Microscopy. *Science* **2009,** *325*, 1110-1114.

[6] Zhao, R.; Zhang, Y.; Gao, T.; Gao, Y.; Liu, N.; Fu, L.; Liu, Z. Scanning tunneling microscope observations of non-AB stacking of graphene on Ni films. *Nano Res.* **2011,** *4*, 712-721.

[7] Li, Z.; Chen, H. Y. T.; Schouteden, K.; Lauwaet, K.; Giordano, L.; Trioni, M. I.; Janssens, E.; Iancu, V.; Van Haesendonck, C.; Lievens, P. et al. Self-Doping of Ultrathin Insulating Films by Transition Metal Atoms. *Phys. Rev. Lett.* **2014,** *112*, 026102.

[8] Repp, J.; Meyer, G.; Stojković, S. M.; Gourdon, A.; Joachim, C. Molecules on Insulating Films: Scanning-Tunneling Microscopy Imaging of Individual Molecular Orbitals. *Phys. Rev. Lett.* **2005,** *94*, 026803.

[9] Repp, J.; Meyer, G.; Paavilainen, S.; Olsson, F. E.; Persson, M. Imaging bond formation between a gold atom and pentacene on an insulating surface. *Science* **2006,** *312*, 1196-1199.

[10] Lin, X.; Nilius, N.; Freund, H. J.; Walter, M.; Frondelius, P.; Honkala, K.; Häkkinen, H. Quantum Well States in Two-Dimensional Gold Clusters on MgO Thin Films. *Phys. Rev. Lett.* **2009,** *102*, 206801.

[11] Repp, J.; Meyer, G.; Olsson, F. E.; Persson, M. Controlling the charge state of individual gold adatoms. *Science* **2004,** *305*, 493-495.

[12] Olsson, F. E.; Paavilainen, S.; Persson, M.; Repp, J.; Meyer, G. Multiple Charge States of Ag Atoms on Ultrathin NaCl Films. *Phys. Rev. Lett.* **2007,** *98*, 176803.

[13] Loth, S.; Lutz, C. P.; Heinrich, A. J. Spin-polarized spin excitation spectroscopy. *New J. Phys.* **2010,** *12*, 125021.

[14] Novaes, F. D.; Lorente, N.; Gauyacq, J.-P. Quenching of magnetic excitations in single adsorbates at surfaces: Mn on CuN/Cu(100). *Phys. Rev. B* **2010,** *82*, 155401.

[15] Loth, S.; Baumann, S.; Lutz, C. P.; Eigler, D. M.; Heinrich, A. J. Bistability in Atomic-Scale Antiferromagnets. *Science* **2012,** *335*, 196-199.

[16] Hebenstreit, W.; Redinger, J.; Horozova, Z.; Schmid, M.; Podloucky, R.; Varga, P. Atomic resolution by STM on ultra-thin films of alkali halides: experiment and local density calculations. *Surf. Sci.* **1999,** *424*, L321-L328.

[17] Repp, J.; Fölsch, S.; Meyer, G.; Rieder, K.-H. Ionic Films on Vicinal Metal Surfaces: Enhanced Binding due to Charge Modulation. *Phys. Rev. Lett.* **2001,** *86*, 252-255.

[18] Repp, J.; Meyer, G.; Rieder, K.-H. Snell's Law for Surface Electrons: Refraction of an Electron Gas Imaged in Real Space. *Phys. Rev. Lett.* **2004,** *92*, 036803.

[19] Repp, J.; Meyer, G.; Paavilainen, S.; Olsson, F. E.; Persson, M. Scanning Tunneling Spectroscopy of Cl Vacancies in NaCl Films: Strong Electron-Phonon Coupling in Double-Barrier Tunneling Junctions. *Phys. Rev. Lett.* **2005,** *95*, 225503.

[20] Lauwaet, K.; Schouteden, K.; Janssens, E.; Haesendonck, C. V.; Lievens, P. Dependence of the NaCl/Au(111) interface state on the thickness of the NaCl layer. *J. Phys.: Condens. Matter* **2012,** *24*, 475507.

[21] Olsson, F. E.; Persson, M.; Repp, J.; Meyer, G. Scanning tunneling microscopy and spectroscopy of NaCl overlayers on the stepped Cu(311) surface:Experimental and theoretical study. *Phys. Rev. B* **2005,** *71*, 075419.

[22] Lauwaet, K.; Schouteden, K.; Janssens, E.; Van Haesendonck, C.; Lievens, P.; Trioni, M. I.; Giordano, L.; Pacchioni, G. Resolving all atoms of an alkali halide via nanomodulation of the thin NaCl film surface using the Au(111) reconstruction. *Phys. Rev. B* **2012,** *85*, 245440.

[23] Schouteden, K.; Lauwaet, K.; Janssens, E.; Barcaro, G.; Fortunelli, A.; Van Haesendonck, C.; Lievens, P. Probing the atomic structure of metallic nanoclusters with the tip of a scanning tunneling microscope. *Nanoscale* **2014,** *6*, 2170-2176.

[24] Cheng, Z.; Du, S.; Guo, W.; Gao, L.; Deng, Z.; Jiang, N.; Guo, H.; Tang, H.; Gao, H. J. Direct imaging of molecular orbitals of metal phthalocyanines on metal surfaces with an O_2-functionalized tip of a scanning tunneling microscope. *Nano Res.* **2011,** *4*, 523-530.

[25] Horcas, I.; Fernandez, R.; Gomez-Rodriguez, J. M.; Colchero, J.; Gomez-Herrero, J.; Baro, A. M. WSXM: A software for scanning probe microscopy and a tool for nanotechnology. *Rev. Sci. Instrum.* **2007,** *78*, 013705-8.

[26] Hla, S.-W. Scanning tunneling microscopy single atom/molecule manipulation and its application to nanoscience and technology. *J. Vac. Sci. Technol. B* **2005,** *23*, 1351-1360.

[27] Hagelaar, J. H. A.; Flipse, C. F. J.; Cerdá, J. I. Modeling realistic tip structures: Scanning tunneling microscopy of NO adsorption on Rh(111). *Phys. Rev. B* **2008,** *78*, 161405.

[28] Cerdá, J.; Van Hove, M. A.; Sautet, P.; Salmeron, M. Efficient method for the simulation of STM images. I. Generalized Green-function formalism. *Phys. Rev. B* **1997,** *56*, 15885-15899.

[29] Janta-Polczynski, B. A.; Cerda, J. I.; Ethier-Majcher, G.; Piyakis, K.; Rochefort, A. Parallel scanning tunneling microscopy imaging of low dimensional nanostructures. *J. Appl. Phys.* **2008,** *104*, 023702-8.

[30] Cerdá, J.; Soria, F. Accurate and transferable extended Hückel-type tight-binding parameters. *Phys. Rev. B* **2000,** *61*, 7965-7971.

[31] Cerdá, J.; Yoon, A.; Van Hove, M. A.; Sautet, P.; Salmeron, M.; Somorjai, G. A. Efficient method for the simulation of STM images. II. Application to clean Rh(111) and Rh(111)+c(4×2)-2S. *Phys. Rev. B* **1997,** *56*, 15900-15918.

[32] Chen, W.; Madhavan, V.; Jamneala, T.; Crommie, M. F. Scanning Tunneling Microscopy Observation of an Electronic Superlattice at the Surface of Clean Gold. *Phys. Rev. Lett.* **1998,** *80*, 1469-1472.

[33] Kichin, G.; Weiss, C.; Wagner, C.; Tautz, F. S.; Temirov, R. Single Molecule and Single Atom Sensors for Atomic Resolution Imaging of Chemically Complex Surfaces. *J. Am. Chem. Soc.* **2011,** *133*, 16847-16851.

[34] Krenner, W.; Kuhne, D.; Klappenberger, F.; Barth, J. V. Assessment of scanning tunneling spectroscopy modes inspecting electron confinement in surface-confined supramolecular networks. *Scientific reports* **2013,** *3*, 1454.

[35] Schouteden, K.; Li, Z.; Iancu, V.; Muzychenko, D. A.; Janssens, E.; Lievens, P.; Van Haesendonck, C. Engineering the Band Structure of Nanoparticles by an Incommensurate Cover Layer. *J. Phys. Chem. C* **2014,** *118*, 18271-18277.